Antiviral Activity of Nrf2 in a Murine Model of Respiratory Syncytial Virus Disease

Hye-Youn Cho[1], Farhad Imani[1], Laura Miller-DeGraff[1], Dianne Walters[1], Guillermina A. Melendi[2,3], Masayuki Yamamoto[4], Fernando P. Polack[2,3], and Steven R. Kleeberger[1]

[1]Laboratory of Respiratory Biology, National Institute of Environmental Health Sciences, National Institutes of Health, Research Triangle Park, North Carolina; [2]Department of Pediatrics, Johns Hopkins University School of Medicine, Baltimore, Maryland; [3]INFANT Foundation, Buenos Aires, Argentina; [4]Tohoku University Graduate School of Medicine, Sendai, Japan

Rationale: Respiratory syncytial virus (RSV) is the most frequent cause of significant lower respiratory illness in infants and young children, but its pathogenesis is not fully understood. The transcription factor Nrf2 protects lungs from oxidative injury and inflammation via antioxidant response element (ARE)-mediated gene induction.
Objectives: The current study was designed to determine the role of Nrf2-mediated cytoprotective mechanisms in murine airway RSV disease.
Methods: Nrf2-deficient ($Nrf2^{-/-}$) and wild-type ($Nrf2^{+/+}$) mice were intranasally instilled with RSV or vehicle. In a separate study, $Nrf2^{+/+}$ and $Nrf2^{-/-}$ mice were treated orally with sulforaphane (an Nrf2-ARE inducer) or phosphate-buffered saline before RSV infection.
Measurements and Main Results: RSV-induced bronchopulmonary inflammation, epithelial injury, and mucus cell metaplasia as well as nasal epithelial injury were significantly greater in $Nrf2^{-/-}$ mice than in $Nrf2^{+/+}$ mice. Compared with $Nrf2^{+/+}$ mice, significantly attenuated viral clearance and IFN-γ, body weight loss, heightened protein/lipid oxidation, and AP-1/NF-κB activity along with suppressed antioxidant induction was found in $Nrf2^{-/-}$ mice in response to RSV. Sulforaphane pretreatment significantly limited lung RSV replication and virus-induced inflammation in $Nrf2^{+/+}$ but not in $Nrf2^{-/-}$ mice.
Conclusions: The results of this study support an association of oxidant stress with RSV pathogenesis and a key role for the Nrf2-ARE pathway in host defense against RSV.

Keywords: airway; oxidative stress; antioxidant response element; inflammation; sulforaphane

Respiratory syncytial virus (RSV) is a seasonal ubiquitous airway pathogen that infects high-risk groups, including infants and young children as well as immune compromised adults and the elderly worldwide; most (>95%) children are known to be infected by the virus by age 2 (1). RSV infection is associated with severe lower respiratory illness characterized by bronchiolitis and respiratory failure and is the leading cause of infant hospitalization (2).

Severe RSV disease is associated with increased virus titers in the lungs leading to epithelial damage and sloughing, mucus production, and augmented inflammation linked to decreased Th1 and increased Th2 cytokine production (3, 4). Extensive research on host immune responses to RSV has been conducted

AT A GLANCE COMMENTARY

Scientific Knowledge on the Subject

Respiratory syncytial virus (RSV) remains the leading cause of severe lower airway disease in infants and in susceptible adults. Although extensive clinical and animal studies have been directed to RSV recently, the mechanisms of susceptibility and etiology remain unclear.

What This Study Adds to the Field

RSV pathogenesis is implicated with oxidative stress, and the Nrf2-directed pathway contributes to host protection against RSV. Suppressed RSV disease phenotypes by an Nrf2 inducer suggest a potential therapeutic strategy for susceptible individuals.

in humans and in laboratory animals, and roles for innate immune receptors, including toll-like receptor 4 (5), chemokines such as Cx3cl1 (6), Th1 IFN-γ (7) and Th2 IL-4 (8) cytokines, and intracellular adhesion molecule-1 (9), have been suggested in RSV pathogenesis. However, details of molecular mechanisms underlying RSV disease are not well understood.

Recent studies have demonstrated that reactive oxygen species (ROS) production and lipid peroxidation may implicate RSV toxicity to lung cells and tissues (10–13). Antioxidant treatment has been suggested to provide some protection against RSV disease (14). Because airway epithelial cells are the major source of antioxidant enzymes/defense proteins are the primary targets for RSV, it is important to determine the role of cellular antioxidant mechanisms in RSV pathogenesis. Transcriptional activation of antioxidant/defense enzymes is mainly through binding of Nrf2 to antioxidant response elements (AREs) on their 5′ promoter. A protective role of the Nrf2-ARE pathway has been examined in experimental models of pulmonary disorders caused by various oxidants and inflammatory agents (15–20). In these studies, suppression or lack of ARE-driven antioxidant expression in mice genetically deficient in Nrf2 ($Nrf2^{-/-}$) has exacerbated lung inflammation and injury compared with wild types ($Nrf2^{+/+}$). However, the role for Nrf2 in host viral infection has not been determined.

The current study was designed to test the hypothesis that Nrf2- and ARE-driven downstream mechanisms play a protective role in airway RSV pathogenesis in mice. For this purpose, we determined lung viral loads, upper and lower airway injury and inflammation, molecular and cellular phenotypes, and oxidative stress markers in $Nrf2^{+/+}$ and $Nrf2^{-/-}$ mice infected with RSV. These mice were also orally pretreated with sulforaphane before RSV infection to determine whether activation of the Nrf2-ARE pathway prevents RSV disease. Results from the current studies provide compelling evidence for an impor-

tant regulatory role of Nrf2 as a host defense mechanism against RSV disease. Some of the results of this study have been previously reported in an abstract (21).

METHODS

Animals and Treatment

$Nrf2^{+/+}$ and $Nrf2^{-/-}$ mice (ICR background) were obtained (22) and pathogen-free breeding colonies were maintained at the National Institute of Environmental Health Sciences. Male (6–8 weeks of age) mice were infected with human RSV-A2 strain by intranasal instillation of 10^6 plaque-forming units (PFU) per mouse in 50 μL Hanks' balanced salt solution (HBSS). HBSS containing Hep-2 cell lysates was intranasally instilled into mice for vehicle control. Animals were killed at 1, 3, 5, or 7 days after intranasal exposure (n = 8–13 per group from a duplicated study). In a separate study, mice were treated with R-sulforaphane (1-isothiocyanato-4-(methyl-sulfinyl)butane, 9 μmol in 100 μL PBS per dose) isolated from broccoli (LKT Laboratories, Inc., St. Paul, MN) or with PBS orally three times at 48-hour intervals. One day after the last gavage treatment, mice were intranasally instilled with RSV (10^6 PFU) or vehicle and killed at 1 day after instillation (n = 6 per group from a duplicated study). All mice were provided food (modified AIN-76A) and water *ad libitum*. Constant air temperature (72 ± 3°F) and relative humidity (50 ± 15%) were maintained during the experiments. On designated post instillation days, mice were killed by sodium pentobarbital overdose (104 mg/kg body weight). All animal use was approved by the National Institute of Environmental Health Sciences Animal Care and Use Committee.

Lung Viral Titration

Viral titer was done with right lung lobes following procedures described previously (23). Briefly, the right lung (n = 3/group) was ground in HBSS, debris was pelleted by centrifugation, and samples were plated on Hep-2 cells. Monolayers overlaid were incubated for 5 days, and plates were stained by the immunoperoxidase method.

Bronchoalveolar Lavage Analyses

The right lung of each mouse was lavaged *in situ* four consecutive times with HBSS (0.5 ml/25 g body weight). The bronchoalveolar lavage fluid (BALF) was analyzed for total protein content (a marker of lung permeability) and epithelial and inflammatory cell numbers following the procedure published previously (17).

ELISA for Cytokine Measurement

Cytokines IL-6, IL-10, IL-13, IL-18, and IFN-γ in BALF (20–50 μl) were determined using mouse-specific ELISA kits (R&D Systems, Minneapolis, MN) according to the manufacturer's instructions.
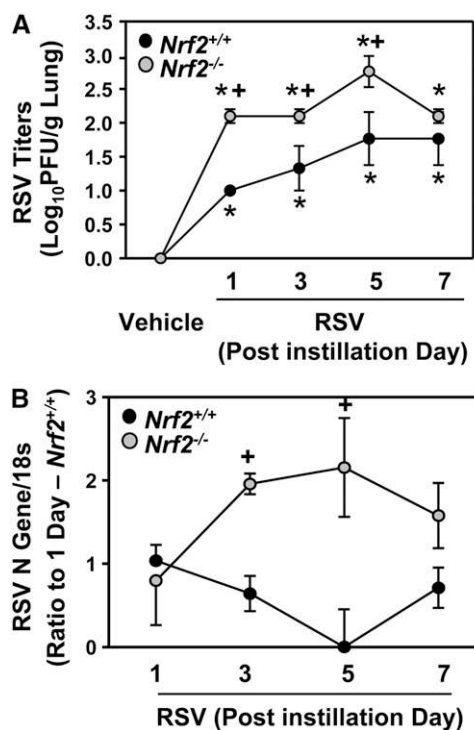
Pulmonary Airway Histopathology

The left lung from each mouse (n = 3–5/group) was inflated intratracheally *in situ* with zinc formalin and fixed following the procedures published previously (24). The fixed lung lobe was sectioned at proximal (around generation 5) and distal (around generation 11) levels of the main axial airway (25), and tissue blocks were embedded in paraffin for preparation of cuts (5 μm) to be stained with hematoxylin and eosin (H&E) for histopathologic analysis and with Alcian Blue (pH 2.5)/periodic acid-Schiff (AB/PAS) reagent to identify acidic and neutral mucosubstances. Severity of pulmonary toxicity determined by microscopic evaluation of H&E-stained slides was assigned into four groups including normal, mild focal, moderate to severe focal injury with areas of normal lung tissue, or severe inflammation and injury (26).
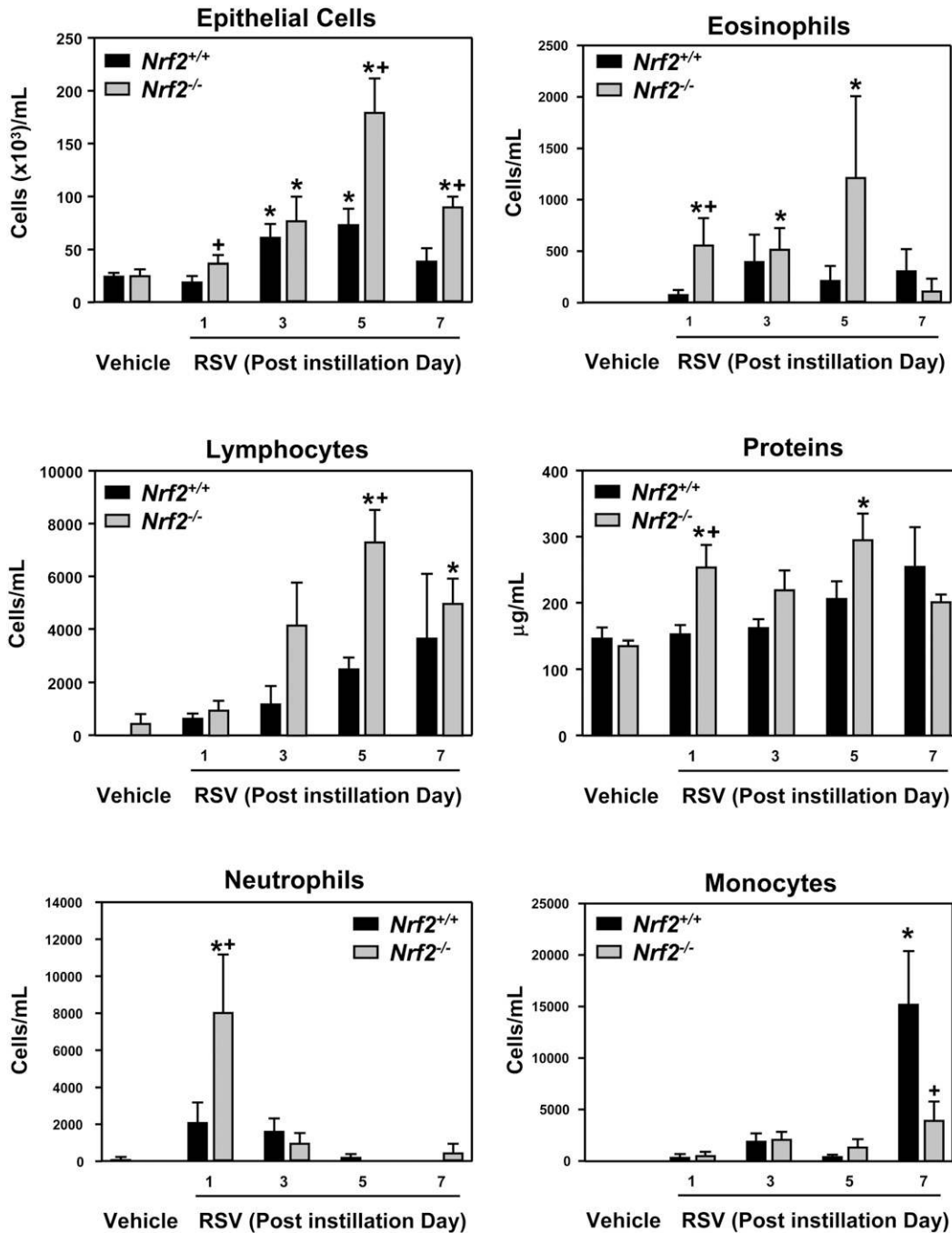
Nasal Airway Analysis

The head of each mouse (n = 5/group) was excised, and retrograde lavage of the nasal airways was performed *in situ* with HBSS (1 ml)

Figure 1. Nrf2 deficiency delayed lung respiratory syncytial virus (RSV) clearance. (*A*) Amount of live RSV in right lung homogenates (n = 3/group) was determined by a plaque-forming assay in $Nrf2^{+/+}$ and $Nrf2^{-/-}$ mice after vehicle or RSV instillation. Data are presented as mean ± SEM. *Significantly different from genotype-matched vehicle mice ($P < 0.05$). +Significantly different from exposure-matched $Nrf2^{+/+}$ mice ($P < 0.05$). (*B*) Replication of the RSV N gene was determined by reverse transcriptase-polymerase chain reaction in $Nrf2^{+/+}$ and $Nrf2^{-/-}$ mice after RSV instillation using vehicle groups as negative controls. Data are presented as means ± SEM of relative expression ratio to the level of 1 day after instillation in $Nrf2^{+/+}$ mice after normalization with 18s rRNA level. *Significantly different from genotype-matched vehicle mice ($P < 0.05$). +Significantly different from exposure-matched $Nrf2^{+/+}$ mice ($P < 0.05$).

TABLE 1. cDNA PRIMER SEQUENCES FOR QUANTITATIVE REVERSE TRANSCRIPTASE-POLYMERASE CHAIN REACTION

Gene Name		Primer Sequences	GeneBank ID	Amplified Sequence (bp)
18s	Forward	TACCTGGTTGATCCTGCCAG	53990	1–184
	Reverse	CCGTCGGCATGTATTAGCTC		
RSV N	Forward	AGATCAACTTCTGTCATCCAGCAA	3089371	1182–1265
	Reverse	TTCTGCACATCATAATTAGGAGTATCAAT		
RSV G	Forward	CGCACCGCTAAGACATTAGA	3089371	4710–4945
	Reverse	CAACCCCAACATACCTCACC		
Nrf2	Forward	ATG GAT TTGATTGACATCCTT	7653877	282–581
	Reverse	AAAGTACAAGGCATCTTGTTT		
GCLc	Forward	ATCAAAGGCTTCTCAGCCAG	1815761	681–880
	Reverse	CAATGTCTGACACGTAGCCT		
NQO1	Forward	AGCGAGCTGG AAAATACTCT	13435425	1141–1303
	Reverse	GGCCATTGTTTACTTTGAGC		
UGT1a6	Forward	ATGTGCCCAGATTCTACACCA	801898	700–945
	Reverse	GGAAGATCATGTTGGGCATGA		
HO-1	Forward	AGATCAGCACTAGCTCATCCC	6754211	901–1074
	Reverse	GCCAGGCAAGATTCTCCCTTA		
GST-P1	Forward	ATGCTGCTGGCTGACCAGGGC	10092607	107–319
	Reverse	CATCTGGGCGGCTCCCTCTG		
GPx2	Forward	GAGGCAGGGCTGTGCTGATT	17432428	211–410
	Reverse	ACCCCCAGGTCGGACATACT		

Figure 2. Nrf2 deficiency augmented pulmonary injury and inflammation by respiratory syncytial virus (RSV). Numbers of epithelial cells, lymphocytes, neutrophils, eosinophils, and monocytes, and total protein concentration were determined by bronchoalveolar lavage fluid (BALF) analysis in $Nrf2^{+/+}$ and $Nrf2^{-/-}$ mice after vehicle or RSV instillation. Data are presented as mean $\pm$ SEM (n = 5 mice/group). *Significantly different from genotype-matched vehicle mice ($P < 0.05$). +Significantly different from exposure-matched $Nrf2^{+/+}$ mice ($P < 0.05$).

through a catheter inserted into the nasopharyngeal orifice. Nasal airway injury was quantified by total cell counts and protein measurement in nasal wash fluid as indicated in BAL analysis. For histopathology, nonlavaged excised heads (n = 3–5/group) were flushed retrograde via a cannula through the nasopharyngeal orifice with zinc formalin, and the fixed heads were processed following the procedures published elsewhere (27, 28) to achieve proximal aspect of the nasal cavity sections. The tissue blocks were embedded in paraffin, and 5-μm-thick section cuts from the anterior face were histologically stained for H&E and AB/PAS. Severity of nasal airway histopathology was evaluated on H&E-stained slides following the same criteria used in pulmonary injury and inflammation as described above.

Reverse Transcriptase-Polymerase Chain Reaction

Total lung RNA isolated from left lung pieces (RNeasy Mini Kit, Qiagen Inc., Valencia CA) was processed for semi-quantitative reverse transcriptase-polymerase chain reaction (RT-PCR) as previously published (17) using gene-specific primers (17, 29). For quantitative PCR, cDNA equivalent to 20 to 50 ng of RNA was amplified in a 25-μl reaction containing 12.5 μl 2X Power SYBR Green Master Mix (Applied Biosystems, Foster City, CA) and 240 nM of each gene-specific forward and reverse primer (Table 1) by 10-minute hold at 95°C and up to 45 cycles of 95°C (15 s) −60°C (1 minute) using an ABI Prism 7700 Sequence Detection System (Applied Biosystems). The relative quantification of gene expression was calculated from the threshold cycle (C_T) values for each sample and normalized in relation to the expression of 18s rRNA using the comparative C_T method.

Lung Protein Isolation

Total lung proteins were prepared from right lung homogenates (n = 3/group) in RIPA buffer including PMSF (10 μg/ml) and protease/phosphatase inhibitor cocktail (Sigma-Aldrich, St. Louis, MO). Nuclear
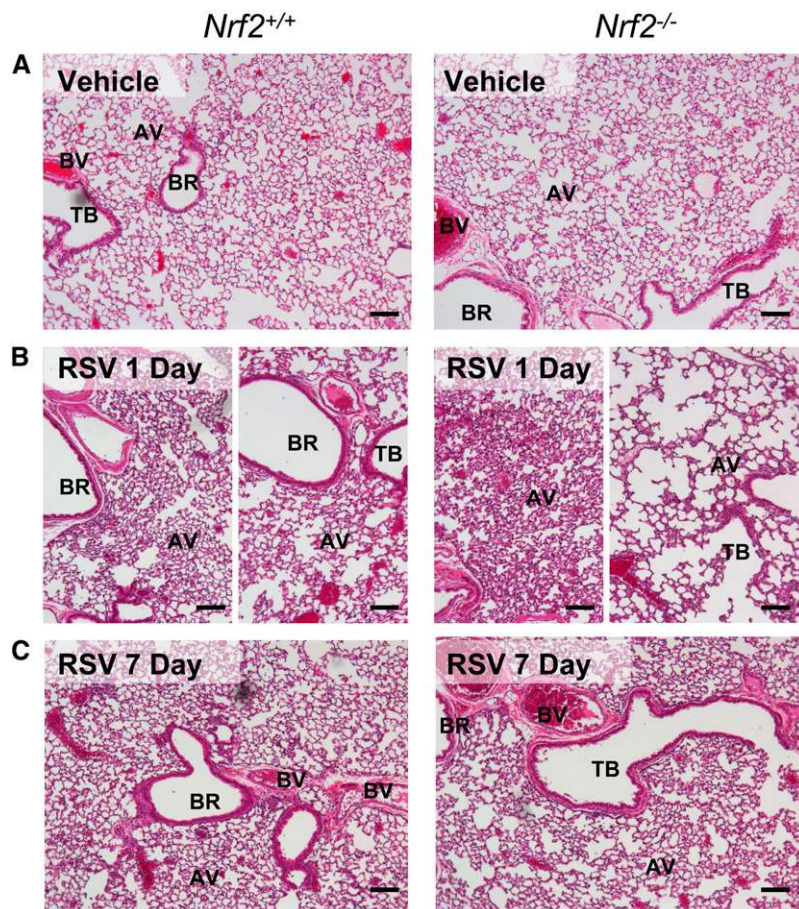
Figure 3. *Nrf2* deficiency exacerbated lung histopathologic phenotypes of respiratory syncytial virus (RSV) infection. Representative light photomicrographs of lung sections from *Nrf2*$^{+/+}$ and *Nrf2*$^{-/-}$ mice (n = 3–5/group) of vehicle controls (*A*) or 1 day (*B*) and 7 days (*C*) after infection stained with H&E. Increased airway cellularity in proximal sections (*left panels*) and loss of alveolar structure in distal sections (*right panels*) was marked in *Nrf2*$^{-/-}$ mice relative to *Nrf2*$^{+/+}$ mice at 1 day. Bronchial and alveolar epithelial proliferation (hyperplasia) and alveolar vacuolization remained more obvious in *Nrf2*$^{-/-}$ mice than in *Nrf2*$^{+/+}$ mice by 7 days. AV = alveoli; BR = bronchi or bronchiole; BV = blood vessel; TB terminal bronchiole. Bars indicate 100 μm.

and cytosolic proteins were isolated from pulverized right lung tissues following the procedure described elsewhere (24). Proteins were quantified and stored in aliquots at −80°C.

Electrophoretic Mobility Shift Assay

Nuclear DNA binding activities of Nrf2, NF-κB, and AP-1 were determined by gel shift analyses of nuclear protein aliquots (3–5 μg) on 3×10^4 cpm [γ^{32}P] ATP end-labeled, double-stranded oligonucleotide containing a consensus binding sequence for ARE, NF-κB, and AP-1, respectively, following the procedure described previously (17). Specific binding activity for small Maf protein was determined by preincubation of nuclear proteins with anti-small Maf (F/K/G) antibody (Santa Cruz Biotechnology, Santa Cruz, CA) for 2 hours in ice followed by electrophoretic mobility shift assay (EMSA).

Western Blot Analyses

Lung total (30–100 μg) or nuclear (10–30 μg) proteins were separated on appropriate percentage Tris-HCl SDS-PAGE gels (Bio-Rad) and analyzed by routine Western blotting using specific antibodies against mucin 5, subtypes A and C (Muc5ac) (Lab Vision Corp., Fremont, CA), Nrf2 (Santa Cruz), γ L-glutamyl cystein ligase (Lab Vision Corp.), NAD(P)H:quinone oxidoreductase 1 (NQO1) (Novus Biologicals, Inc., Littleton, CO), glutathione-S-transferase-P (GST-P) (Abcam, Cambridge, MA), heme oxygenase 1 (HO-1) (Assay Designs, Inc., Ann Arbor, MI), or actin (Santa Cruz). Representative protein blot images from multiple Western blot analyses were scanned by a Bio-Rad Gel Doc system.

Protein Oxidation Detection

Oxidized protein levels were determined in total lung protein aliquots by immunoblot assay of carbonyl groups introduced into protein side chains by oxidative reactions using the OxyBlot Protein Oxidation Detection kit (Upstate/Chemicon, Temecula, CA). Briefly, denatured protein samples (15 μg) were incubated with 2.4-dinitrophenyl hydra-

zine for 15 minutes at room temperature for derivatization. After neutralization of the derivatized protein, samples were loaded on a SDS-PAGE gel for Western blot analysis using an anti-DNP primary antibody and a secondary antibody provided. Separate protein sample aliquots were incubated with derivatization negative control solution and processed for the same immunoblot analysis. For quantification of protein carbonyl derivative levels, total lung protein samples (1 μg in 100 μl volume) and BSA standards (mixture of oxidized/reduced BSA) were adsorbed onto a 96-well plate (OxiSelect Protein Carbonyl ELISA kit; Cell Biolabs, Inc., San Diego, CA) overnight at 4°C. After 2.4-dinitrophenyl hydrazine derivatization of the protein carbonyls present, the protein samples were incubated with an anti-DNP antibody and a horseradish peroxidase–conjugated secondary antibody according to the manufacturer's instructions. The protein carbonyl contents were determined by colorimetric analysis at 450 nm using a standard curve prepared from predetermined reduced and oxidized BSA standards.

Lipid Hydroperoxidation Measurement

Lipid hydroperoxide levels were measured in aliquots of BALF (500 μl from 2nd–4th return fluid) as another marker for oxidative airway injury using the Lipid Hydroperoxide Assay kit (Calbiochem, San Diego, CA). Briefly, lipid hydroperoxides were extracted from BAL samples with chloroform. Ferric ions (Fe^{3+}) generated from the redox reaction of extracted hydroperoxides and ferrous ions (Fe^{2+}) were detected spectrophotometrically (500 nm) as $Fe(SCN)_5^{2-}$ by the addition of a chromogen (SCN).

Lung Glutathione Measurement

The reduced form of glutathione (GSH) was determined in lung RIPA homogenates by a colorimetric method (Northwest Life Science Specialties, LLC, Vancouver, WA). Oxidized glutathione levels were determined by adding a GSH scavenger 4-vinylpyridine (Sigma-Aldrich)
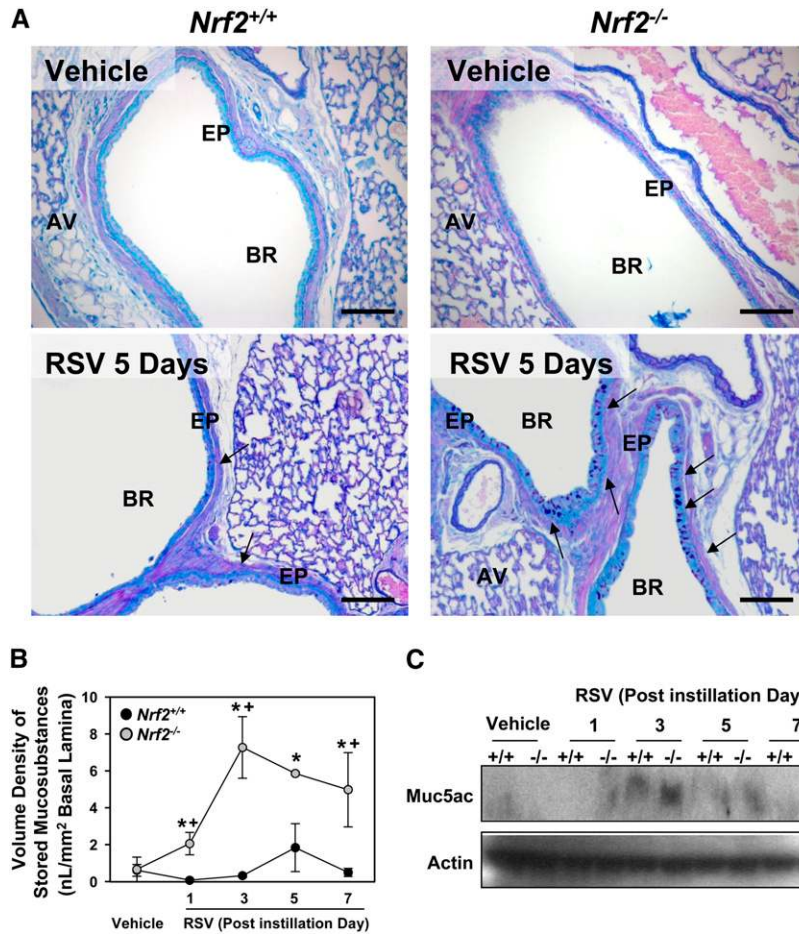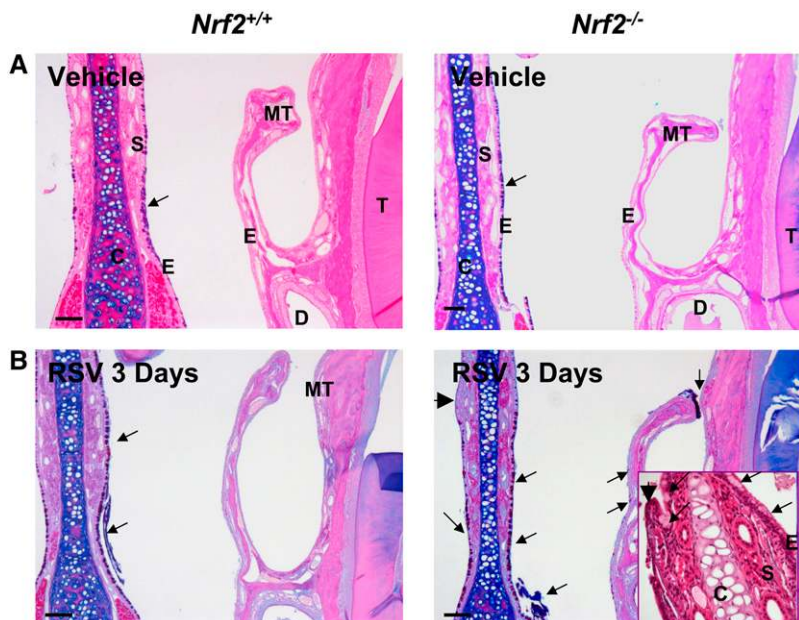
Figure 4. *Nrf2* deficiency augmented lung mucous cell metaplasia after respiratory syncytial virus (RSV) infection. (*A*) Representative light photomicrographs (n = 3–5/group) visualize AB/PAS-stained lung sections for intraepithelial mucosubstances, a marker of mucous cell metaplasia, in mice after RSV (5 days). *Arrows* indicate mucosubstances stored in the bronchial epithelium. AV = alveoli; EP = epithelium; BR = bronchi or bronchiole. Bars indicate 100 μm. (*B*) Morphometric measurement of volume density (Vs) of AB/PAS-positive mucosubstances in bronchial epithelium. Data presented as mean ± SEM (n = 3–5/group). *Significantly different from genotype-matched vehicle mice ($P < 0.05$). +Significantly different from exposure-matched *Nrf2*$^{+/+}$ mice ($P < 0.05$). (*C*) Muc5ac protein level in lung homogenates determined by Western blot analysis. Representative digitized images are shown from multiple analyses.

in the reaction (10 mM at final) according to the manufacturer's instructions.

Morphometry of Stored Intraepithelial Mucosubstances

The amount of stored mucosubstances in the bronchial epithelium was estimated as a marker of mucous cell metaplasia using computerized image analysis and standard morphometric techniques (30, 31). Briefly, images of AB/PAS-stained cross-sections from the intrapulmonary axial airway (generation 5 level) in the left lobe were taken using a light microscope with an attached camera (Carl Zeiss MicroImaging, Inc., Thornwood, NY). The area of AB/PAS-positive mucosubstances within the surface epithelium lining the largest daughter branch and the next generation bronchioles was calculated from the semiautomatically

Figure 5. *Nrf2* deficiency enhanced respiratory syncytial virus (RSV)-induced nasal airway injury. Representative light photomicrographs (n = 3–5/group) of AB/PAS staining depicted acidic and neutral mucosubstances in *Nrf2*$^{+/+}$ and *Nrf2*$^{-/-}$ mice after vehicle (*A*) and RSV infection (*B*, 3 days). RSV caused greater mucus hypersecretion to air space and focal mucous cell hyperplasia in mucosal epithelium of mid-septum as well as mild mucous cell metaplasia in the epithelium lining maxilloturbinates in *Nrf2*$^{-/-}$ than in *Nrf2*$^{+/+}$ mice. Higher magnification of midseptum stained with H&E elucidated respiratory epithelial lesions manifest by abnormal epithelial differentiation and goblet cell proliferation in *Nrf2*$^{-/-}$ mice infected with RSV. *Arrows* indicate AB/PAS-stained intraepithelial or secreted mucosubstances. *Arrowheads* indicate focal injury sites. C = cartilage; E = epithelium; MT = maxilloturbinate; S = septum. Bars indicate 100 μm.

TABLE 2. NASAL LAVAGE ANALYSIS OF TOTAL PROTEIN EDEMA AND CELLULAR INJURY IN NASAL AIRWAYS CAUSED BY VEHICLE AND RESPIRATORY SYNCYTIAL VIRUS (1 D AFTER INSTILLATION).*

Nasal Airway Phenotypes	Exposure	$Nrf2^{+/+}$	$Nrf2^{-/-}$
Total proteins, μg/ml	Vehicle	116 ± 44	157 ± 13
	RSV	347 ± 33[†]	652 ± 209[†]
Total cells, ×10³/ml	Vehicle	4 ± 1	7 ± 4
	RSV	23 ± 3[†]	62 ± 29[†]

Definition of abbreviation: RSV = respiratory syncytial virus.
* Data are presented as group means ± SEM (n = 5 mice/group).
[†] Significantly different from genotype-matched vehicle control mice ($P < 0.05$).

circumscribed perimeter of the stained material using Scion Image software (Scion Corporation, Frederick, MD). The length of the basal lamina underlying the surface epithelium was concomitantly calculated from the contour length on the digitized images using the same system. The volume of intraepithelial mucosubstances per unit surface area (volume density [Vs] nl/mm² basal lamina) was determined as previously described (32, 33).

Statistics

Data were expressed as the group mean ± SEM. For the time course study, two-way analysis of variance (ANOVA) was used to evaluate the effects of exposure (vehicle, RSV postinstillation times) and genotype ($Nrf2^{+/+}$, $Nrf2^{-/-}$). One-way ANOVA was used for Nrf2 mRNA assessment in $Nrf2^{+/+}$ mice. For the pretreatment study, three-way ANOVA was used to evaluate the effects of genotype ($Nrf2^{+/+}$, $Nrf2^{-/-}$), pretreatment (PBS, sulforaphane), and exposure (vehicle, RSV). The Student-Newman-Keuls test was used for *a posteriori* comparisons of means ($P < 0.05$). All of the statistical analyses were performed using the SigmaStat 3.0 software program (SPSS Science Inc., Chicago, IL).

RESULTS

Delayed Viral Clearance, Potentiated Viral Replication, and Enhanced Body Weight Loss in $Nrf2^{-/-}$ Mice

Lung RSV titers peaked 5 days after infection in both strains (Figure 1A). RSV titers in $Nrf2^{-/-}$ mice were significantly

higher (tenfold) than those in $Nrf2^{+/+}$ mice 1 to 5 days after instillation (Figure 1A). Compared with $Nrf2^{+/+}$ mice, significantly higher viral N (Figure 1B) and G (data not shown) gene replication was found in the lungs of $Nrf2^{-/-}$ mice at 3 and 5 days. Neither virus nor viral gene was detected in the lungs of vehicle control mice. A statistically significant ($P < 0.001$) $Nrf2$ effect on body weight loss caused by RSV infection relative to respective vehicle control mice was found. Weight loss relative to time-matched vehicle controls was significantly greater in $Nrf2^{-/-}$ mice compared with $Nrf2^{+/+}$ mice at days 3 (−0.97 ± 0.54% versus 1.2 ± 0.45%) and 5 (−1.82 ± 1.10% versus 0.275 ± 0.55%) after RSV infection.

### Augmentation of Bronchoalveolar Injury and Inflammation in $Nrf2^{-/-}$ Mice

Relative to respective vehicle controls, RSV significantly increased the numbers of epithelial cells and lymphocytes (from 3 days) in BALF from $Nrf2^{+/+}$ and $Nrf2^{-/-}$ mice. RSV-induced increases in the numbers of epithelial cells (5–7 days) and lymphocytes (5 days) were significantly higher in $Nrf2^{-/-}$ mice than in $Nrf2^{+/+}$ mice. RSV infection also significantly increased the total protein concentration and numbers of neutrophils and eosinophils over the vehicle only in $Nrf2^{-/-}$ mice. The numbers of monocytes were significantly increased by RSV in $Nrf2^{+/+}$ mice at 7 days but not in $Nrf2^{-/-}$ mice (Figure 2).

Exacerbation of Lung Histopathologic Phenotypes in $Nrf2^{-/-}$ Mice

Mice treated with vehicle had no significant histopathologic changes in their lungs (Figure 3A). One day after RSV, H&E-stained lung sections indicated that airway epithelium lining the first daughter branch (bronchi) was partially exfoliated, and mild to moderate (in $Nrf2^{+/+}$) or moderate to severe (in $Nrf2^{-/-}$) inflammatory cell infiltration was marked in alveoli and proximal airways (Figure 3B). Alveolar vacuolization and loss of alveolar structure was more prevalent in $Nrf2^{-/-}$ than in $Nrf2^{+/+}$ mice in distal sections of the lung (Figure 3B). Beginning at day 3, perivascular and peribronchiolar lymphocyte patches appeared in both strains of mice consistent with significant
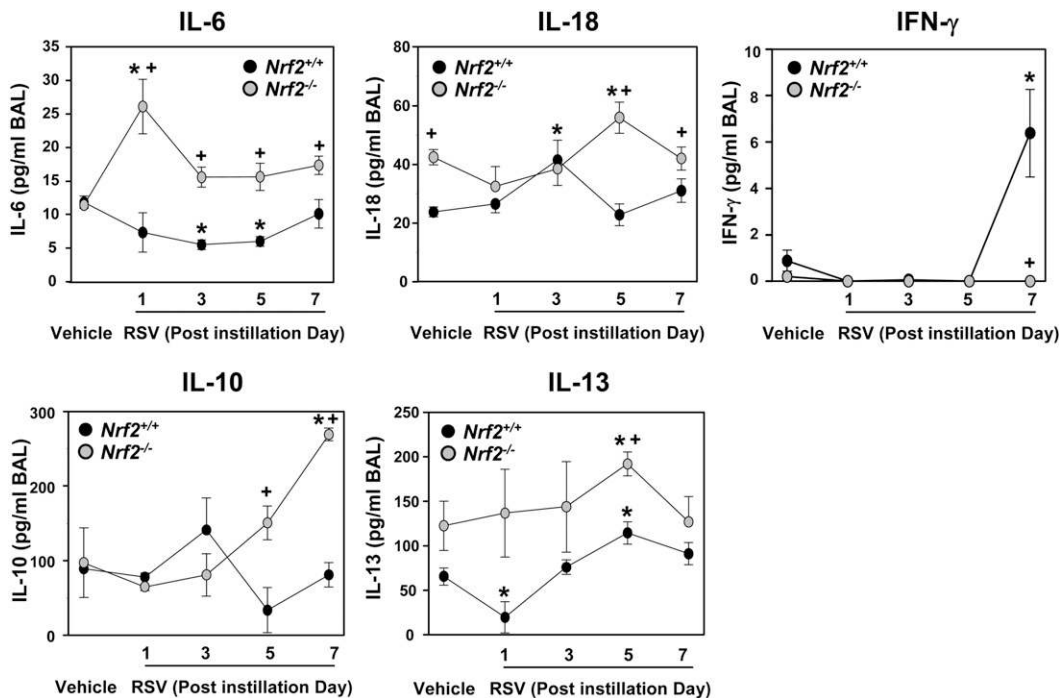
Figure 6. Differential increase of pulmonary cytokines in $Nrf2^{+/+}$ and $Nrf2^{-/-}$ mice after respiratory syncytial virus (RSV) infection. Bronchoalveolar lavage (BAL) fluid levels of IL-6, IL-10, IL-13, IL-18, and IFN-γ in $Nrf2^{+/+}$ and $Nrf2^{-/-}$ mice instilled with vehicle or RSV were determined by ELISA. Data are presented as group mean ± SEM (n = 3/group). *Significantly different from genotype-matched vehicle mice ($P < 0.05$). [+]Significantly different from exposure-matched $Nrf2^{+/+}$ mice ($P < 0.05$).
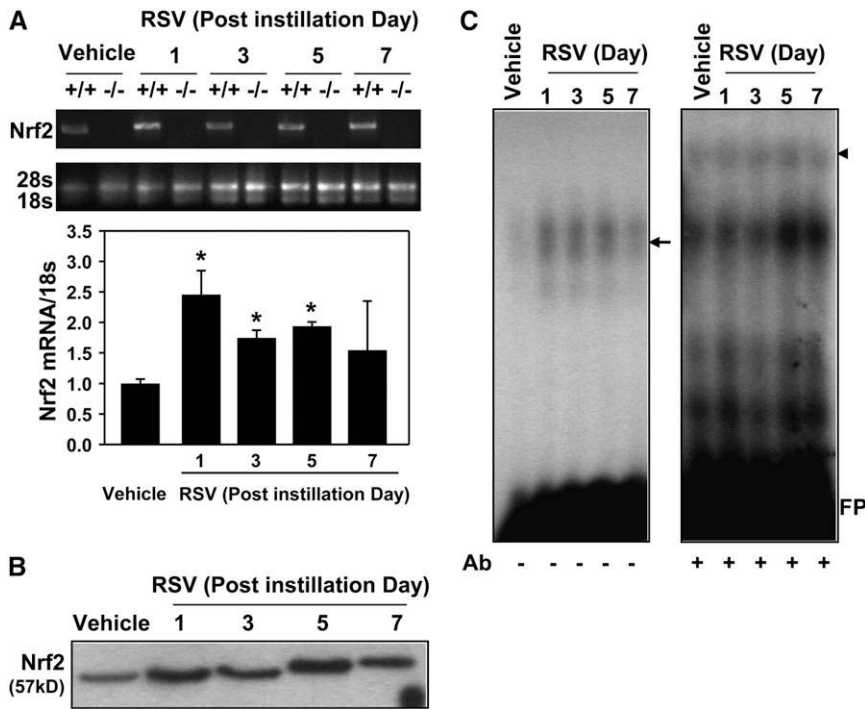
Figure 7. Respiratory syncytial virus (RSV)-induced up-regulation and activation of lung Nrf2 in $Nrf2^{+/+}$ mice. (*A*) Representative digitized image from semi-quantitative reverse transcriptase-polymerase chain reaction (RT-PCR) demonstrates increased Nrf2 mRNA expression in $Nrf2^{+/+}$ mice. 18s rRNA bands are shown as matching internal controls. Quantitative RT-PCR assessed the relative ratio of Nrf2 cDNA levels over the vehicle controls after normalization to corresponding 18s rRNA levels. Data are presented as the normalized group mean $\pm$ SEM (n = 3/group). *Significantly different from vehicle control mice ($P < 0.05$). (*B*) Western blot analysis of lung nuclear proteins from $Nrf2^{+/+}$ mice determined that RSV exposure increased nuclear translocation of Nrf2 indicated by enhanced intensity of 57-kD bands after RSV. Representative digitized bands from multiple analyses (n = 2/group) are presented. (*C*) Nuclear protein–antioxidant response element (ARE) binding activity was determined by EMSA using an aliquot of nuclear protein from $Nrf2^{+/+}$ mice. Increased total ARE-nuclear protein binding activity was determined by enhanced intensity of shifted bands (*arrow, left panel*). Specific binding activity of small Maf (MafF/G/K), an Nrf2 heterodimer partner for ARE binding, was detected as the appearance of supershifted bands (*arrowhead*) by adding anti-small Maf antibody in the reaction mixture (+Ab, *right panel*). Representative images from separate analyses are presented. FP = free probes.

increases in BAL lymphocytes (*see* Figure 2); the patches persisted through 7 days and were more evident in $Nrf2^{-/-}$ than in $Nrf2^{+/+}$ mice. At 3 and 5 days, hyperplastic changes were developed in airway epithelium lining bronchi, bronchioles, and alveoli in both strains, and this epithelial hyperplasia was more marked in $Nrf2^{-/-}$ than in $Nrf2^{+/+}$ mice (Figure 4A). Most of the RSV-induced pathologic features including alveolar vacuolization and hyperplasia remained in $Nrf2^{-/-}$ mice, whereas they were resolved in $Nrf2^{+/+}$ mice by 7 days after instillation (Figure 3C).

Bronchial epithelium lining the large-diameter main axial airways and air space of proximal left lung sections contained AB/PAS-stained mucosubstances in both strains infected with RSV, which were rarely found in normal airways (Figure 4A). These markers of mucous (goblet) cell metaplasia concurrent with mucus hypersecretion and epithelial hyperplasia appeared as early as 1 day with a peak at 3 to 5 days in both strains and were more evident in $Nrf2^{-/-}$ than in $Nrf2^{+/+}$ mice (Figure 4A). Morphometric quantification determined a significant increase (3- to 11-fold) of stored intraepithelial mucosubstances (Vs) from 1 to 7 days in $Nrf2^{-/-}$ mice, whereas Vs in $Nrf2^{+/+}$ mice was not significantly increased after RSV infection (Figure 4B). The increase of the predominant airway mucin core protein Muc5ac was also higher in $Nrf2^{-/-}$ mice than in $Nrf2^{+/+}$ mice at 1 to 5 days (Figure 4C).

Severe Histopathologic Injury in Nasal Airways of $Nrf2^{-/-}$ Mice

Vehicle caused little histopathologic alteration in the nasal passages of either strain. The main histologic lesions caused by RSV were present in respiratory epithelium lining the proximal nasal airways. Compared with vehicle controls (Figure 5A), moderate to severe inflammatory cell infiltration was evident in blood vessels, septum, and surface epithelium lining the nasal septum of RSV-infected mice from 1 day. Nasal lavage analysis identified significant peak injury phenotypes at 1 day with increased total protein and total cell numbers; however,

no statistically significant genotype effect was found in these parameters (Table 2). RSV-induced changes in nasal airway histopathology were most obvious at 3 days in both strains, and more severe epithelial damage was found in $Nrf2^{-/-}$ than in $Nrf2^{+/+}$ mice (Figure 5B). Prominent pathologic features in $Nrf2^{-/-}$ mice were mucus hypersecretion, mucous cell hyperplasia in the mid-septal epithelium, and mucous cell metaplasia in the epithelium lining maxilloturbinates (Figure 5B). Severe epithelial alterations were also found in the mid-septum or in the dorsal maxilloturbinates of $Nrf2^{-/-}$ mice, which includes epithelial exfoliation, proliferation (hyperplasia), or transformation into unusual cell types presumed to be focal squamous cell metaplasia (Figure 5B).

Differential Pulmonary Cytokine Profiles after RSV Infection

BAL IL-6 levels, determined as an inflammatory parameter of innate immunity, were significantly elevated in $Nrf2^{-/-}$ mice over controls at 1 day after instillation and were greater in $Nrf2^{-/-}$ mice than in $Nrf2^{+/+}$ mice at all times after RSV infection (Figure 6). Compared with vehicle controls, IL-6 level in $Nrf2^{+/+}$ mice was significantly decreased (3 and 5 days) after viral infection. IL-18, a potential mediator for orchestrating Th1 and/or Th2 immune responses to RSV infection, was determined. Constitutive BAL IL-18 concentration was significantly higher in $Nrf2^{-/-}$ mice than in $Nrf2^{+/+}$ mice, and IL-18 was significantly more elevated by RSV in $Nrf2^{-/-}$ mice than in $Nrf2^{+/+}$ mice after 5 days. BAL concentrations of the Th1 cytokine IFN-γ in $Nrf2^{+/+}$ mice were not significantly increased relative to controls until 7 days after RSV infection as shown in previous kinetic studies of murine RSV models (7, 34), but lung IFN-γ was not significantly increased at any time in $Nrf2^{-/-}$ mice. Among BAL Th2 cytokines, IL-10 was not significantly changed in $Nrf2^{+/+}$ mice but was significantly elevated in $Nrf2^{-/-}$ mice at 7 days. IL-13 was significantly increased at 5 days after RSV in both genotypes but was significantly higher in $Nrf2^{-/-}$ mice than in $Nrf2^{+/+}$ mice.
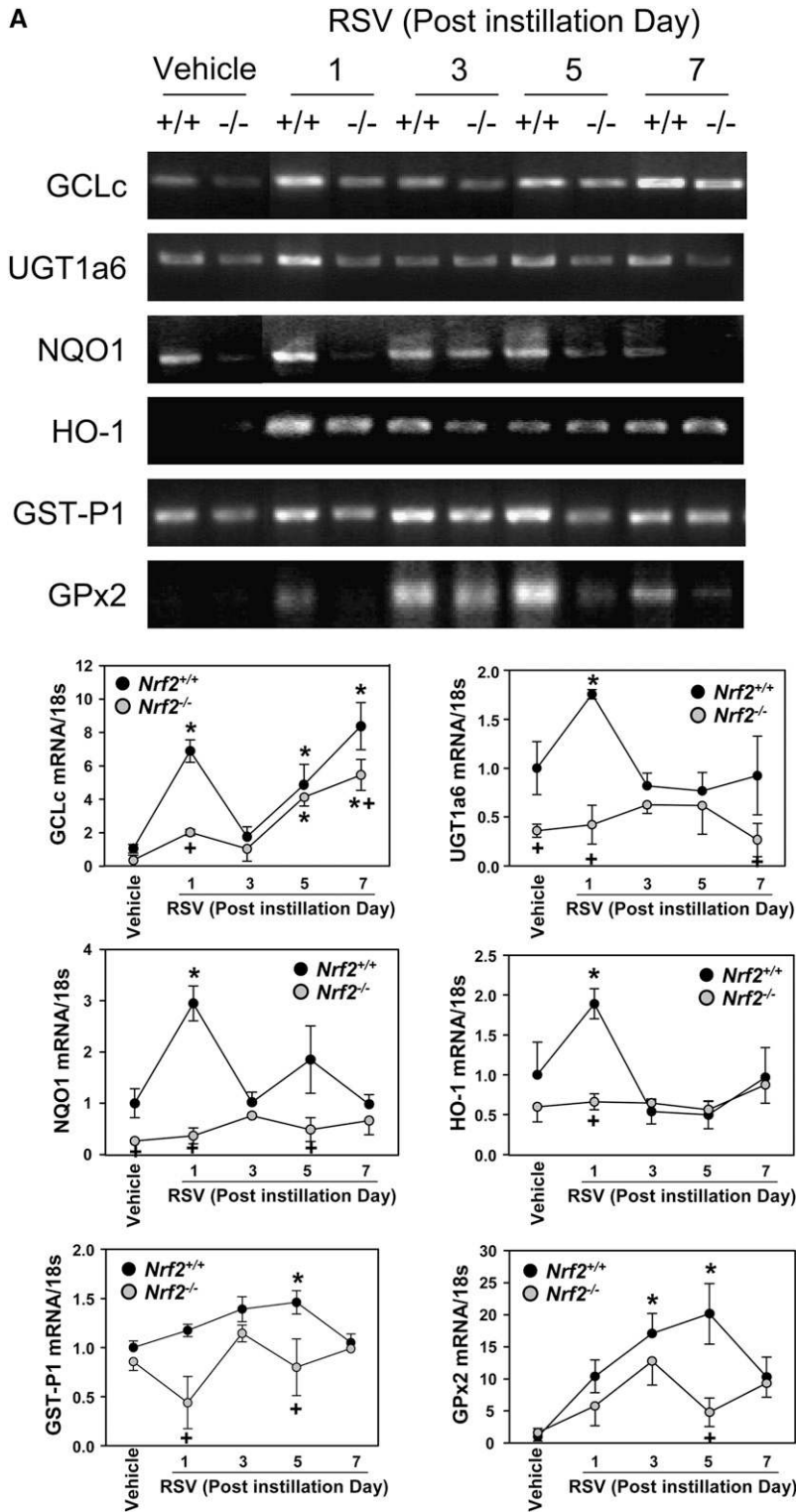
Figure 8. Suppression of antioxidant response element (ARE)-responsive antioxidant/detoxifying enzyme induction by RSV in $Nrf2^{-/-}$ mice. (*A*) Expression of pulmonary ARE-driven antioxidant genes determined by reverse transcriptase-polymerase chain reaction (RT-PCR) analysis. Representative digitized image from semi-quantitative RT-PCR demonstrates increased Nrf2 and ARE-driven antioxidant mRNA expression. Quantitative RT-PCR assessed the relative ratio of each cDNA levels over $Nrf2^{+/+}$-vehicle control after normalization to corresponding 18s rRNA levels, and data presented in graphs are the normalized group mean $\pm$ SEM (n = 3/group). *Significantly different from genotype-matched vehicle control mice ($P < 0.05$). $^+$Significantly different from exposure-matched $Nrf2^{+/+}$ mice ($P < 0.05$). (*B*) Western blot analyses of lung total proteins from $Nrf2^{+/+}$ and $Nrf2^{-/-}$ mice determined Nrf2-dependent protein expression of pulmonary antioxidant/detoxifying enzymes after RSV infection. Actin levels are shown as internal controls. Representative digitized bands from multiple analyses (n = 3/group) are presented.

Activation of Pulmonary Nrf2 in $Nrf2^{+/+}$ Mice

Steady-state Nrf2 mRNA expression was significantly (2.5-fold) increased by RSV in the lungs of $Nrf2^{+/+}$ mice by 1 day and remained significantly elevated by 5 days (Figure 7A). Enhanced nuclear translocation of Nrf2 protein was found in the lungs from 1 day after RSV (Figure 7B). Functional analysis for DNA binding activity by electrophoretic mobility shift assay (EMSA) demonstrated that RSV infection promoted nuclear total ARE binding activity (shifted bands, arrow on left panel) in the lungs of $Nrf2^{+/+}$ mice (Figure 7C). Specific ARE binding activity of small Maf (F/G/K), the heterodimeric partner of Nrf2 for ARE binding, was also enhanced by RSV in $Nrf2^{+/+}$ mice (Figure 7C, supershifted bands indicated as an arrow head on right panel). Overall, RSV caused activation of pulmonary Nrf2 through mRNA induction, nuclear translocation, and increased ARE binding in $Nrf2^{+/+}$ mice.
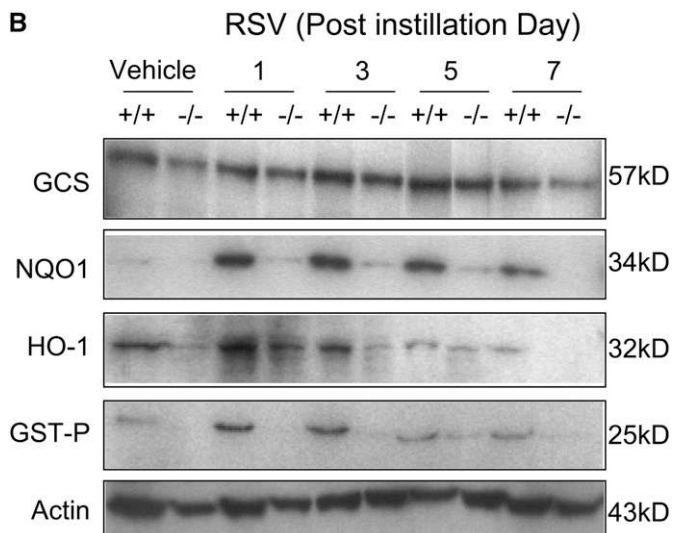
Figure 8. (*continued*)

Suppression of ARE-Responsive Antioxidant Induction in *Nrf2*$^{-/-}$ Mice

RSV caused significant transcriptional and translational induction of multiple ARE-bearing antioxidant/defense enzymes, catalytic subunit (GCLc) of γ L-glutamyl cystein ligase, UDP glucuronyl transferase (UGT) 1a6, NQO1, HO-1, GST-P1, and glutathione peroxidase 2 (GPx2). Steady state mRNA levels for GCLc, NQO1, and HO-1 were significantly elevated at or from 1 day, whereas GST-P1 and GPx2 mRNA expressions were significantly higher over the controls at 3 or 5 days after RSV (Figure 8A). Protein levels of the examined antioxidant enzymes were also elevated over the vehicle controls at 1 to 7 days in *Nrf2*$^{+/+}$ mice (Figure 8A). Message and protein induction of these lung defense enzymes were significantly or completely attenuated in *Nrf2*$^{-/-}$ mice compared with *Nrf2*$^{+/+}$ mice after RSV infection (Figure 8A, 8B).

Heightened Oxidative Stress in *Nrf2*$^{-/-}$ Mice

Glutathione levels. Basal lung level of GSH was significantly lower in *Nrf2*$^{-/-}$ mice than in *Nrf2*$^{+/+}$ mice. RSV infection significantly diminished GSH in *Nrf2*$^{-/-}$ and *Nrf2*$^{+/+}$ mice in a time-dependent manner, and GSH level was significantly lower in *Nrf2*$^{-/-}$ than in *Nrf2*$^{+/+}$ mice at 1 and 3 days. Oxidized glutathione (GSSG) was significantly enhanced by RSV after 3 days in *Nrf2*$^{+/+}$ mice, whereas no significant changes were found in *Nrf2*$^{-/-}$ mice after RSV. Overall, the lung glutathione pool was significantly depleted in *Nrf2*$^{-/-}$ mice, and utilization (oxidation) of GSH to counteract oxidative stress caused by RSV was also suppressed in *Nrf2*$^{-/-}$ mice compared with *Nrf2*$^{+/+}$ mice (Figure 9A).

Lung protein and lipid oxidation. The magnitude of lung oxidative stress was estimated by measuring oxidation of endogenous macromolecules, proteins, and lipids. Oxidatively modified protein bands were detected at 45 to 60 kD in *Nrf2*$^{-/-}$ mice but not in *Nrf2*$^{+/+}$ mice after vehicle treatment (Figure 9B). After RSV infection, the intensity and number of protein oxidation bands (30–70 kD) were time-dependently elevated in both genotypes (Figure 9B). Quantified protein oxidation levels were significantly greater (20–25%) in *Nrf2*$^{-/-}$ mice than in *Nrf2*$^{+/+}$ mice at all times (Figure 9B). Relative to vehicle controls, significant increases in BAL lipid hydroperoxides were detected 7 days after RSV infection in both strains (Figure 9C) but were significantly higher in *Nrf2*$^{-/-}$ mice than in *Nrf2*$^{+/+}$ mice (Figure 9C).

Redox-sensitive transcription factors. Baseline binding activity of lung nuclear AP-1 was slightly higher in *Nrf2*$^{-/-}$ mice over *Nrf2*$^{+/+}$ mice (Figure 9D). After RSV infection, no significant change of AP-1 binding activity was found in *Nrf2*$^{+/+}$ mice (Figure 9D). In *Nrf2*$^{-/-}$ mice (Figure 9D), AP-1 activity was increased at 1 and 3 days after instillation (Figure 9D). Similar to AP-1, nuclear NF-κB binding activity in *Nrf2*$^{+/+}$ mice changed minimally, whereas binding activity in *Nrf2*$^{-/-}$ mice increased after viral infection (Figure 9D).

Inhibition of Viral Replication and Lung Inflammation by Sulforaphane Pretreatment in *Nrf2*$^{+/+}$ Mice

In PBS-treated mice infected with RSV, lung viral replication determined by G gene abundance was not significantly different between two genotypes as depicted in Figure 1B (Figure 10A). However, sulforaphane treatment significantly decreased RSV gene expression level in *Nrf2*$^{+/+}$ mice relative to *Nrf2*$^{-/-}$ mice (Figure 10A). RSV genes were not detected in vehicle groups. A constitutive level of Nrf2 message and nuclear Nrf2 protein was enhanced in mice by pretreatment with sulforaphane in *Nrf2*$^{+/+}$ mice (Figure 10B). After RSV infection, transcription and nuclear translocation of Nrf2 was highly activated, although the elevated mRNA and nuclear protein level did not differ between PBS- and sulforaphane-treated groups (Figure 10B). Sulforaphane treatment increased basal message levels of multiple ARE-bearing antioxidants including NQO1, GST-P1, HO-1, and GPx2 in *Nrf2*$^{+/+}$ mice, whereas the effect of sulforaphane was negligible in *Nrf2*$^{-/-}$ mice (Figure 10C). After RSV infection, the message level for these antioxidants was similar (GST-P1) or lower (other genes) in sulforaphane-treated *Nrf2*$^{+/+}$ mice compared with PBS-treated *Nrf2*$^{+/+}$ mice, indicating that the fortified antioxidative environment by sulforaphane lowered oxidative stress caused by virus infection in these mice (Figure 10C). RSV-induced antioxidant gene expression was highly suppressed in all the experimental groups of *Nrf2*$^{-/-}$ mice compared with corresponding *Nrf2*$^{+/+}$ mice as quantified in the time-course study shown in Figure 8A (Figure 10C). Significantly reduced numbers of BAL neutrophils and eosinophils were observed after sulforaphane pretreatment in *Nrf2*$^{+/+}$ mice infected with RSV (Figure 10D). However, RSV-induced neutrophilic and eosinophilic inflammation in *Nrf2*$^{-/-}$ mice was not significantly resolved by sulforaphane (Figure 10D). Overall, pretreatment with sulforaphane significantly reduced RSV load and virus-induced early pulmonary inflammation in *Nrf2*$^{+/+}$ mice, whereas a significant sulforaphane effect was not observed in *Nrf2*$^{-/-}$ mice in response to RSV.

DISCUSSION

The current study demonstrated that the Nrf2-ARE pathway plays a protective role in murine airways against RSV-induced injury and oxidative stress. Compared with *Nrf2*$^{+/+}$ mice, more severe RSV disease, including higher viral titers, augmented inflammation, and enhanced mucus production and epithelial injury were found in *Nrf2*$^{-/-}$ mice. Supporting the role for Nrf2, pretreatment with a potent Nrf2-ARE inducer in *Nrf2*$^{+/+}$ mice significantly attenuated pulmonary viral load and early inflammation after RSV infection. Results of this investigation are the first to demonstrate an important role for Nrf2-mediated cytoprotective mechanisms in host viral infection and suggest a potential means for intervention.

Recent studies have shown that RSV infection enhanced production of ROS (e.g., superoxide anions, hydrogen peroxides, lipid peroxides) in lavaged inflammatory cells or in cultured airway cells (10–13), which suggested a role for oxidative stress
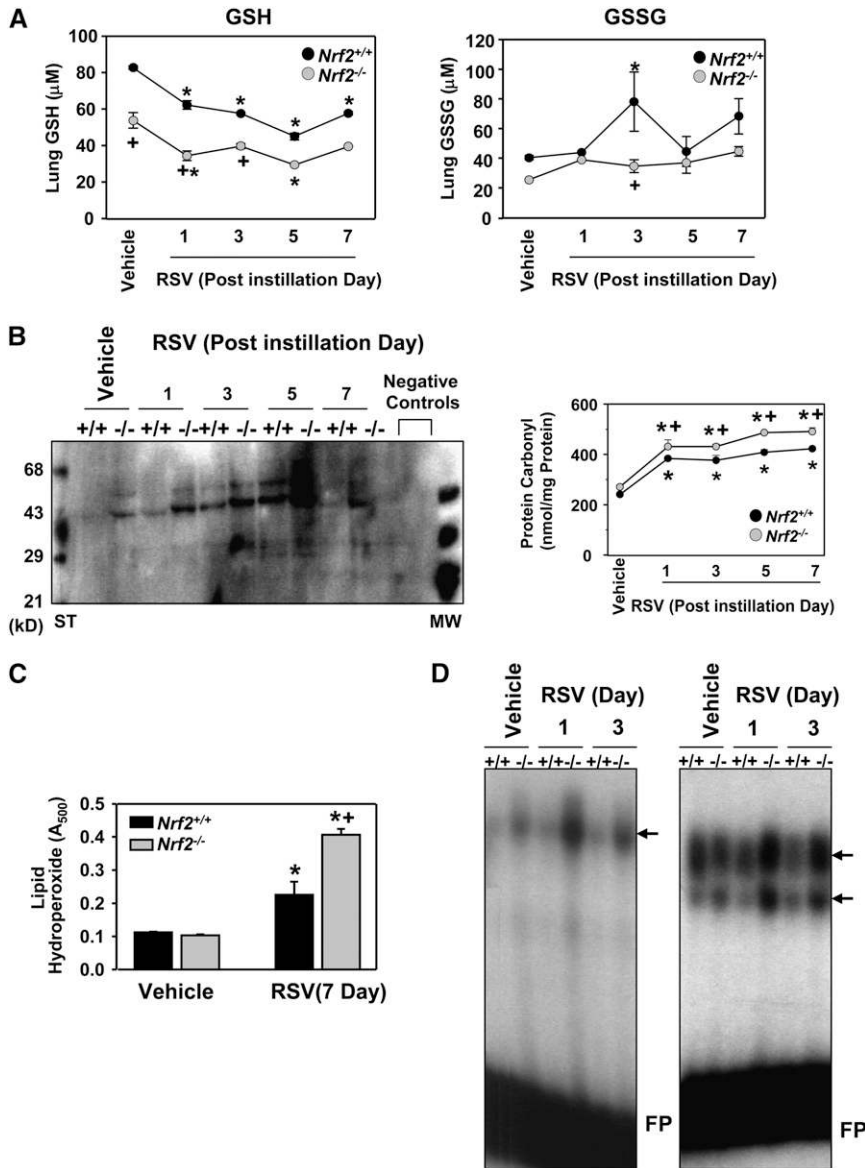
Figure 9. *Nrf2* deficiency enhanced lung oxidative stress markers after respiratory syncytial virus (RSV) infection. (*A*) Reduced (GSH) and oxidized (GSSG) forms of glutathione levels in lung homogenates. Data are presented as mean ± SEM (n = 3/group). *Significantly different from genotype-matched vehicle control mice ($P < 0.05$). +Significantly different from exposure-matched $Nrf2^{+/+}$ mice ($P < 0.05$). (*B*) Protein oxidation level determined by immunoblotting for carbonyl moieties introduced in lung proteins using an anti-dinitrophenyl (DNP) antibody. Oxidatively modified proteins appeared mostly at 30 to 70 kD, and the intensities were increased in $Nrf2^{-/-}$ mice in a time-dependent manner. ST = derivatized protein standard; MW = normal molecular markers. Negative controls indicate nonderivatized lung protein samples. Protein carbonyl derivative level was quantified in total lung lysates (1 μg) by a colorimetric ELISA kit using an anti-DNP antibody at 450 nm. Data are presented as mean ± SEM (n = 3/group). *Significantly different from genotype-matched vehicle control mice ($P < 0.05$). +Significantly higher than RSV-exposed $Nrf2^{+/+}$ mice ($P < 0.05$). (*C*) Magnitude of lipid oxidation quantified by a colorimetric analysis for lipid hydroperoxides in BALF from $Nrf2^{+/+}$ and $Nrf2^{-/-}$ mice exposed to vehicle or RSV (7 d). Data are presented as mean ± SEM (n = 3/group). *Significantly different from genotype-matched vehicle control mice ($P < 0.05$). +Significantly different from RSV-exposed $Nrf2^{+/+}$ mice ($P < 0.05$). (*D*) RSV-induced changes in pulmonary DNA-binding activity of nuclear AP-1 (*left panel*) and NF-κB (*right panel*) was determined by differential intensity of shifted bands (*arrows*) from EMSA. Representative digitized images from separate analyses are presented. FP = free probes.

in RSV pathogenesis. Although phosphorylational activation of STATs 1 and 3 were known to be involved in ROS signal transduction caused by RSV (11), details of molecular and cellular mechanisms underlying airway oxidative stress by RSV have not been elucidated. In the present study, we found that RSV infection caused pulmonary oxidative stress indicated by decreased GSH level and enhanced oxidative modification of proteins and lipids. Nrf2 expression and activity as well as downstream ARE-responsive genes were also highly induced in response to RSV. Castro *et al.* (14) recently demonstrated that treatment with butylated hydroxyanisole (BHA) inhibited RSV-induced inflammation and enhanced viral clearance in murine lungs. Inasmuch as BHA is known to induce the Nrf2-ARE pathway (35), the collective observations indicate the importance of Nrf2-mediated cellular antioxidant mechanisms in pulmonary anti-RSV activity.

Severe RSV disease associated with enhanced viral titer in $Nrf2^{-/-}$ mice resulted in augmented airway inflammation, and pretreatment with sulforaphane reversed these critical phenotypes in mice with intact *Nrf2*. RSV-induced early increase in airway inflammatory cells was likely due to the concurrent activation of redox-sensitive transcription factors, AP-1 and

NF-κB in $Nrf2^{-/-}$ mice, whereas their activation was negligible in $Nrf2^{+/+}$ mice. Enhanced NF-κB and AP-1 activation in the acute phase of infection may mediate innate immune and inflammatory responses via cytokine production such as IL-6 in $Nrf2^{-/-}$ mice. Although details of molecular mechanisms have not been elucidated, Nrf2-mediated negative regulation of inflammatory modulators has been demonstrated in other pulmonary disease models, such as asthma, chronic obstructive pulmonary disorders, and idiopathic pulmonary fibrosis (15, 17–20, 36). Emerging evidence also strongly suggests that the lack of *Nrf2* causes various immune disorders including lupus-like autoimmune syndromes (37, 38), sepsis (39), and inflammatory bowel disease (40, 41). We also evaluated airways reactivity in these mice before and after RSV infection. Airways responses to aerosolized acetylcholine (measured using the Flexivent system) were not significantly different between the wild-type and $Nrf2^{-/-}$ mice at baseline or after RSV infection (data not shown). These results suggest that *Nrf2* deficiency did not significantly affect airway reactivity in response to RSV. The precise mechanisms of induced (allergen, virus, oxidant) or basal airway hyperreactivity are not known, although it is likely that multiple mechanisms can lead to this phenotype. We postulate
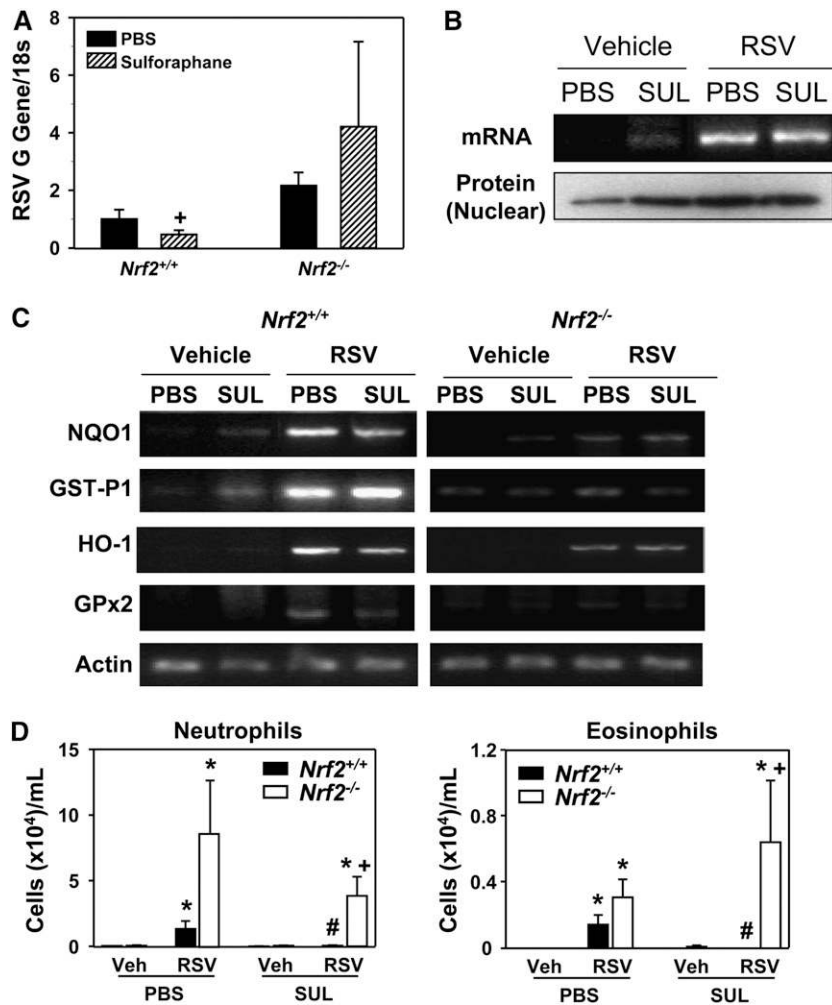
Figure 10. Sulforaphane pretreatment suppressed respiratory syncytial virus (RSV) infection and lung inflammation in $Nrf2^{+/+}$ mice but not in $Nrf2^{-/-}$ mice. (A) Replication of the RSV G gene determined by semiquantitative reverse transcriptase-polymerase chain reaction (RT-PCR) in $Nrf2^{+/+}$ and $Nrf2^{-/-}$ mice 1 day after virus instillation indicated an inhibitory effect of sulforaphane on viral load in $Nrf2^{+/+}$ but not in $Nrf2^{-/-}$ mice. Total lung RNA from vehicle-exposed mice was used as a negative control. Data are presented as mean ± SEM (n = 3/group) of the relative expression ratio to the level 1 day after instillation in phosphate buffered saline–treated RSV-exposed $Nrf2^{+/+}$ mice after normalization with individual 18s rRNA level. +Significantly different from exposure-matched (sulforaphane-treated, RSV-instilled) $Nrf2^{-/-}$ mice ($P < 0.05$). (B) Nrf2 message and nuclear protein levels in $Nrf2^{+/+}$ mice presented by representative images (n = 3/group) from RT-PCR and Western blotting analysis, respectively. Sulforaphane (SUL) pretreatment increased Nrf2 transcription and nuclear translocation relative to PBS at baseline (vehicle), whereas no additive effects of sulforaphane were found on Nrf2 activation after RSV infection. (C) Representative images (n = 3/group) for mRNA expression of pulmonary ARE-driven antioxidant enzymes determined by semiquantitative RT-PCR analyses in $Nrf2^{+/+}$ and $Nrf2^{-/-}$ mice pretreated with PBS or SUL after vehicle or RSV exposure (1 day). Actin mRNA levels are shown as internal controls. (D) Protective effect of SUL pretreatment on RSV-induced inflammation determined by BAL analysis for neutrophils and eosinophils in $Nrf2^{+/+}$ but not in $Nrf2^{-/-}$ mice after 1 day of RSV. Data are presented as mean ± SEM (n = 3/vehicle instilled groups, n = 6/RSV instilled groups). *Significantly different from genotype- and pretreatment-matched vehicle control (Veh) mice ($P < 0.05$). +Significantly different from sulforaphane-treated RSV-exposed $Nrf2^{+/+}$ mice ($P < 0.05$). #Significantly different from PBS-treated RSV-exposed $Nrf2^{+/+}$ mice ($P < 0.05$).

that the background strain of the mice used in this study (ICR) may be a contributing factor inasmuch as ICR mice behaved more like Th1-responders as determined by relatively lower pulmonary eosinophilia and serum IgE induction along with a mild increase of airway hyperreactivity after RSV infection compared with Th2-responder Balbc/J mice, which have been widely used in most of the previous studies of RSV and airways reactivity. However, changes in airways reactivity and inflammation/injury are not always codependent. For example, ozone-induced inflammation in rodents (42) and in human subjects (43, 44) does not necessarily correlate with changes in airways reactivity.

Consistent with our current findings, several previous studies determined that the reduced form of glutathione (GSH) was depleted in $Nrf2^{-/-}$ mice or $Nrf2$-null cells constitutively and under stress conditions (39, 45, 46) due to attenuated synthesis and recycling enzymes for thiols (glutathione, thioredoxin). Alterations in pulmonary thiol metabolism are widely recognized as a central feature of many chronic inflammatory lung diseases. Cellular thiol level has also been suggested as a key factor in Th1 and Th2 response patterns (47, 48). That is, increased GSH/GSSH ratio (relatively reduced condition) directs Th1 skewing with elevation of IFN-γ as naive Th0 cells differentiate preferentially to Th1 cells. Our observation fits with this concept because $Nrf2^{+/+}$ mice, which had relatively higher GSH levels than $Nrf2^{-/-}$ mice, were more "Th1-like" (as indicated by higher IFN-γ) than $Nrf2^{-/-}$ mice, which were more "Th2-like" (as indicated by higher IL-10 and IL-13 than

$Nrf2^{+/+}$ mice) against RSV infection. This is important because Th1 cells are known to contribute to virus clearance, whereas Th2 cells mediate airway eosinophilia, mucus production, and allergic responses (49). Particularly in the clinical situation of RSV infection, many studies demonstrated that the Th1/Th2 cytokine balance in the serum of children with severe RSV disease was more skewed toward Th2 cytokines (4). In addition, IFN-γ has been determined as a dominant host response factor for RSV clearance clinically and in animal studies (7, 50). Therefore, a lack of IFN-γ and Th2-skewed cytokine profile in $Nrf2^{-/-}$ mice may explain their delayed viral clearance and support the enhanced RSV susceptibility.

Our data demonstrate a strong association of ROS-antioxidant mechanisms in RSV pathogenesis. We therefore asked whether induction of Nrf2 and related antioxidant enzymes before RSV infection would ameliorate injury. Sulforaphane is a naturally occurring isothiocyanate found in broccoli. Based on its potent antioxidant enzyme induction properties, accumulating evidence from numerous epidemiologic and laboratory investigations have suggested that it may reduce the risk of cancer and many common chronic degenerative diseases (51–56). The cytoprotective effect of sulforaphane occurs mainly by stabilizing Nrf2 via inhibition of the cytoplasmic Nrf2 inhibitor Keap1 (57–59). Sulforaphane is also known to act through mitogen-activated kinase activation (60), NF-κB inhibition (61), and apoptosis signaling (62, 63). We found that pretreatment with sulforaphane induced elevation of lung ARE-driven antioxidant levels in control (nondisease) conditions, which led to

significantly reduced viral gene replication and lung inflammation against RSV infection. The relatively lower levels of pulmonary antioxidant gene and proteins in sulforaphane-treated mice than in PBS-treated ones after RSV indicate that activated Nrf2-ARE antioxidant defense prevents oxidative stress by subsequent host viral infection. Although not investigated in the present study, the action of sulforaphane through other pathways (e.g., NF-κB inhibition) may also contribute to protection from RSV.

In conclusion, mice with ablated *Nrf2* had significantly greater RSV disease phenotypes compared with mice with intact *Nrf2*, and RSV disease was prevented by pretreatment with an Nrf2 inducer. Our study demonstrated that Nrf2-ARE–mediated antioxidant pathways have a pivotal role in airway cytoprotection and rescue mice from RSV by up-regulation of antioxidants, potentiation of viral clearance, and disregulation of inflammatory mediators. The results of this study indicate that targeting oxidative stress may limit pulmonary RSV infectivity and suggest a potential novel therapeutic means for RSV disease.

References

1. Foy HM, Cooney MK, Maletzky AJ, Grayston JT. Incidence and etiology of pneumonia, croup and bronchiolitis in preschool children belonging to a prepaid medical care group over a four-year period. *Am J Epidemiol* 1973;97:80–92.
2. Hall CB. Respiratory syncytial virus: a continuing culprit and conundrum. *J Pediatr* 1999;135:2–7.
3. Moore ML, Peebles RS Jr. Respiratory syncytial virus disease mechanisms implicated by human, animal model, and in vitro data facilitate vaccine strategies and new therapeutics. *Pharmacol Ther* 2006;112:405–424.
4. Becker Y. Respiratory syncytial virus (RSV) evades the human adaptive immune system by skewing the Th1/Th2 cytokine balance toward increased levels of Th2 cytokines and ige, markers of allergy: a review. *Virus Genes* 2006;33:235–252.
5. Kurt-Jones EA, Popova L, Kwinn L, Haynes LM, Jones LP, Tripp RA, Walsh EE, Freeman MW, Golenbock DT, Anderson LJ, *et al.* Pattern recognition receptors TLR4 and CD14 mediate response to respiratory syncytial virus. *Nat Immunol* 2000;1:398–401.
6. Tripp RA, Jones LP, Haynes LM, Zheng H, Murphy PM, Anderson LJ. Cx3c chemokine mimicry by respiratory syncytial virus G glycoprotein. *Nat Immunol* 2001;2:732–738.
7. van Schaik SM, Obot N, Enhorning G, Hintz K, Gross K, Hancock GE, Stack AM, Welliver RC. Role of interferon gamma in the pathogenesis of primary respiratory syncytial virus infection in Balb/c mice. *J Med Virol* 2000;62:257–266.
8. Boelen A, Kwakkel J, Barends M, de Rond L, Dormans J, Kimman T. Effect of lack of interleukin-4, interleukin-12, interleukin-18, or the interferon-gamma receptor on virus replication, cytokine response, and lung pathology during respiratory syncytial virus infection in mice. *J Med Virol* 2002;66:552–560.
9. Behera AK, Matsuse H, Kumar M, Kong X, Lockey RF, Mohapatra SS. Blocking intercellular adhesion molecule-1 on human epithelial cells decreases respiratory syncytial virus infection. *Biochem Biophys Res Commun* 2001;280:188–195.
10. Casola A, Burger N, Liu T, Jamaluddin M, Brasier AR, Garofalo RP. Oxidant tone regulates rantes gene expression in airway epithelial cells infected with respiratory syncytial virus: role in viral-induced interferon regulatory factor activation. *J Biol Chem* 2001;276:19715–19722.
11. Liu T, Castro S, Brasier AR, Jamaluddin M, Garofalo RP, Casola A. Reactive oxygen species mediate virus-induced stat activation: role of tyrosine phosphatases. *J Biol Chem* 2004;279:2461–2469.
12. Stark JM, Stark MA, Colasurdo GN, LeVine AM. Decreased bacterial clearance from the lungs of mice following primary respiratory syncytial virus infection. *J Med Virol* 2006;78:829–838.
13. Tachibana A, Kimura H, Kato M, Nako Y, Kozawa K, Morikawa A. Respiratory syncytial virus enhances the expression of CD11b molecules and the generation of superoxide anion by human eosinophils primed with platelet-activating factor. *Intervirology* 2002;45:43–51.
14. Castro SM, Guerrero-Plata A, Suarez-Real G, Adegboyega PA, Colasurdo GN, Khan AM, Garofalo RP, Casola A. Antioxidant treatment ameliorates respiratory syncytial virus-induced disease and lung inflammation. *Am J Respir Crit Care Med* 2006;174:1361–1369.
15. Iizuka T, Ishii Y, Itoh K, Kiwamoto T, Kimura T, Matsuno Y, Morishima Y, Hegab AE, Homma S, Nomura A, *et al.* Nrf2-deficient mice are highly susceptible to cigarette smoke-induced emphysema. *Genes Cells* 2005;10:1113–1125.
16. Aoki Y, Sato H, Nishimura N, Takahashi S, Itoh K, Yamamoto M. Accelerated DNA adduct formation in the lung of the Nrf2 knockout mouse exposed to diesel exhaust. *Toxicol Appl Pharmacol* 2001;173:154–160.
17. Cho HY, Jedlicka AE, Reddy SP, Kensler TW, Yamamoto M, Zhang LY, Kleeberger SR. Role of Nrf2 in protection against hyperoxic lung injury in mice. *Am J Respir Cell Mol Biol* 2002;26:175–182.
18. Cho HY, Reddy SP, Yamamoto M, Kleeberger SR. The transcription factor Nrf2 protects against pulmonary fibrosis. *FASEB J* 2004;18:1258–1260.
19. Rangasamy T, Cho CY, Thimmulappa RK, Zhen L, Srisuma SS, Kensler TW, Yamamoto M, Petrache I, Tuder RM, Biswal S. Genetic ablation of Nrf2 enhances susceptibility to cigarette smoke-induced emphysema in mice. *J Clin Invest* 2004;114:1248–1259.
20. Rangasamy T, Guo J, Mitzner WA, Roman J, Singh A, Fryer AD, Yamamoto M, Kensler TW, Tuder RM, Georas SN, *et al.* Disruption of Nrf2 enhances susceptibility to severe airway inflammation and asthma in mice. *J Exp Med* 2005;202:47–59.
21. Cho H-Y, Miller-Degraff L, Imani F, Polack FP, Yamamoto M, Kleeberger SR. Nrf2 deficiency augmented airway injury caused by respiratory syncytial virus infection. *Am J Respir Crit Care Med* 2007;175:A774.
22. Itoh K, Chiba T, Takahashi S, Ishii T, Igarashi K, Katoh Y, Oyake T, Hayashi N, Satoh K, Hatayama I, *et al.* An Nrf2/small maf heterodimer mediates the induction of phase II detoxifying enzyme genes through antioxidant response elements. *Biochem Biophys Res Commun* 1997;236:313–322.
23. Polack FP, Irusta PM, Hoffman SJ, Schiatti MP, Melendi GA, Delgado MF, Laham FR, Thumar B, Hendry RM, Melero JA, *et al.* The cysteine-rich region of respiratory syncytial virus attachment protein inhibits innate immunity elicited by the virus and endotoxin. *Proc Natl Acad Sci USA* 2005;102:8996–9001.
24. Cho HY, Morgan DL, Bauer AK, Kleeberger SR. Signal transduction pathways of tumor necrosis factor–mediated lung injury induced by ozone in mice. *Am J Respir Crit Care Med* 2007;175:829–839.
25. Farraj AK, Harkema JR, Kaminski NE. Allergic rhinitis induced by intranasal sensitization and challenge with trimellitic anhydride but not with dinitrochlorobenzene or oxazolone in A/J mice. *Toxicol Sci* 2004;79:315–325.
26. Johansen HK, Espersen F, Cryz SJ Jr, Hougen HP, Fomsgaard A, Rygaard J, Hoiby N. Immunization with pseudomonas aeruginosa vaccines and adjuvant can modulate the type of inflammatory response subsequent to infection. *Infect Immun* 1994;62:3146–3155.
27. Young JT. Histopathologic examination of the rat nasal cavity. *Fundam Appl Toxicol* 1981;1:309–312.
28. Cho HY, Hotchkiss JA, Harkema JR. Inflammatory and epithelial responses during the development of ozone-induced mucous cell metaplasia in the nasal epithelium of rats. *Toxicol Sci* 1999;51:135–145.
29. Cho HY, Reddy SP, Debiase A, Yamamoto M, Kleeberger SR. Gene expression profiling of Nrf2-mediated protection against oxidative injury. *Free Radic Biol Med* 2005;38:325–343.
30. Hotchkiss JA, Harkema JR, Henderson RF. Effect of cumulative ozone exposure on ozone-induced nasal epithelial hyperplasia and secretory metaplasia in rats. *Exp Lung Res* 1991;17:589–600.
31. Gordon T, Harkema JR. Mucous cell metaplasia in the airways of rats exposed to machining fluids. *Fundam Appl Toxicol* 1995;28:274–282.
32. Heidsiek JG, Hyde DM, Plopper CG, St George JA. Quantitative histochemistry of mucosubstance in tracheal epithelium of the macaque monkey. *J Histochem Cytochem* 1987;35:435–442.
33. Harkema JR, Plopper CG, Hyde DM, St George JA, Dungworth DL. Effects of an ambient level of ozone on primate nasal epithelial mucosubstances: quantitative histochemistry. *Am J Pathol* 1987;127:90–96.
34. Davis IC, Lazarowski ER, Hickman-Davis JM, Fortenberry JA, Chen FP, Zhao X, Sorscher E, Graves LM, Sullender WM, Matalon S. Leflunomide prevents alveolar fluid clearance inhibition by respiratory syncytial virus. *Am J Respir Crit Care Med* 2006;173:673–682.

35. Xu C, Li CY, Kong AN. Induction of phase I, II and III drug metabolism/transport by xenobiotics. *Arch Pharm Res* 2005;28:249–268.

36. Chan K, Kan YW. Nrf2 is essential for protection against acute pulmonary injury in mice. *Proc Natl Acad Sci USA* 1999;96:12731–12736.

37. Yoh K, Itoh K, Enomoto A, Hirayama A, Yamaguchi N, Kobayashi M, Morito N, Koyama A, Yamamoto M, Takahashi S. Nrf2-deficient female mice develop lupus-like autoimmune nephritis. *Kidney Int* 2001;60:1343–1353.

38. Ma Q, Battelli L, Hubbs AF. Multiorgan autoimmune inflammation, enhanced lymphoproliferation, and impaired homeostasis of reactive oxygen species in mice lacking the antioxidant-activated transcription factor Nrf2. *Am J Pathol* 2006;168:1960–1974.

39. Thimmulappa RK, Lee H, Rangasamy T, Reddy SP, Yamamoto M, Kensler TW, Biswal S. Nrf2 is a critical regulator of the innate immune response and survival during experimental sepsis. *J Clin Invest* 2006;116:984–995.

40. Osburn WO, Karim B, Dolan PM, Liu G, Yamamoto M, Huso DL, Kensler TW. Increased colonic inflammatory injury and formation of aberrant crypt foci in Nrf2-deficient mice upon dextran sulfate treatment. *Int J Cancer* 2007;121:1883–1891.

41. Khor TO, Huang MT, Kwon KH, Chan JY, Reddy BS, Kong AN. Nrf2-deficient mice have an increased susceptibility to dextran sulfate sodium-induced colitis. *Cancer Res* 2006;66:11580–11584.

42. Zhang LY, Levitt RC, Kleeberger SR. Differential susceptibility to ozone-induced airways hyperreactivity in inbred strains of mice. *Exp Lung Res* 1995;21:503–518.

43. Balmes JR, Chen LL, Scannell C, Tager I, Christian D, Hearne PQ, Kelly T, Aris RM. Ozone-induced decrements in FEV1 and FVC do not correlate with measures of inflammation. *Am J Respir Crit Care Med* 1996;153:904–909.

44. Uysal N, Schapira RM. Effects of ozone on lung function and lung diseases. *Curr Opin Pulm Med* 2003;9:144–150.

45. Reddy NM, Kleeberger SR, Cho HY, Yamamoto M, Kensler TW, Biswal S, Reddy SP. Deficiency in NRF2-GSH signaling impairs type II cell growth and enhances sensitivity to oxidants. *Am J Respir Cell Mol Biol* 2007;37:3–8.

46. Chan JY, Kwong M. Impaired expression of glutathione synthetic enzyme genes in mice with targeted deletion of the Nrf2 basic-leucine zipper protein. *Biochim Biophys Acta* 2000;1517:19–26.

47. Murata Y, Amao M, Yoneda J, Hamuro J. Intracellular thiol redox status of macrophages directs the Th1 skewing in thioredoxin transgenic mice during aging. *Mol Immunol* 2002;38:747–757.

48. Peterson JD, Herzenberg LA, Vasquez K, Waltenbaugh C. Glutathione levels in antigen-presenting cells modulate Th1 versus Th2 response patterns. *Proc Natl Acad Sci USA* 1998;95:3071–3076.

49. Peebles RS Jr, Graham BS. Pathogenesis of respiratory syncytial virus infection in the murine model. *Proc Am Thorac Soc* 2005;2:110–115.

50. Gern JE, Brooks GD, Meyer P, Chang A, Shen K, Evans MD, Tisler C, Dasilva D, Roberg KA, Mikus LD, *et al.* Bidirectional interactions between viral respiratory illnesses and cytokine responses in the first year of life. *J Allergy Clin Immunol* 2006;117:72–78.

51. Dinkova-Kostova AT, Fahey JW, Wade KL, Jenkins SN, Shapiro TA, Fuchs EJ, Kerns ML, Talalay P. Induction of the phase 2 response in mouse and human skin by sulforaphane-containing broccoli sprout extracts. *Cancer Epidemiol Biomarkers Prev* 2007;16:847–851.

52. Talalay P, Fahey JW. Phytochemicals from cruciferous plants protect against cancer by modulating carcinogen metabolism. *J Nutr* 2001;131:3027S–3033S.

53. Fahey JW, Zhang Y, Talalay P. Broccoli sprouts: an exceptionally rich source of inducers of enzymes that protect against chemical carcinogens. *Proc Natl Acad Sci USA* 1997;94:10367–10372.

54. Shapiro TA, Fahey JW, Dinkova-Kostova AT, Holtzclaw WD, Stephenson KK, Wade KL, Ye L, Talalay P. Safety, tolerance, and metabolism of broccoli sprout glucosinolates and isothiocyanates: a clinical phase I study. *Nutr Cancer* 2006;55:53–62.

55. Dinkova-Kostova AT, Jenkins SN, Fahey JW, Ye L, Wehage SL, Liby KT, Stephenson KK, Wade KL, Talalay P. Protection against UV-light-induced skin carcinogenesis in SKH-1 high-risk mice by sulforaphane-containing broccoli sprout extracts. *Cancer Lett* 2006;240:243–252.

56. Fahey JW, Haristoy X, Dolan PM, Kensler TW, Scholtus I, Stephenson KK, Talalay P, Lozniewski A. Sulforaphane inhibits extracellular, intracellular, and antibiotic-resistant strains of *Helicobacter pylori* and prevents benzo[a]pyrene-induced stomach tumors. *Proc Natl Acad Sci USA* 2002;99:7610–7615.

57. Zhang DD, Hannink M. Distinct cysteine residues in keap1 are required for keap1-dependent ubiquitination of Nrf2 and for stabilization of nrf2 by chemopreventive agents and oxidative stress. *Mol Cell Biol* 2003;23:8137–8151.

58. Jeong WS, Keum YS, Chen C, Jain MR, Shen G, Kim JH, Li W, Kong AN. Differential expression and stability of endogenous nuclear factor E2-related factor 2 (Nrf2) by natural chemopreventive compounds in HepG2 human hepatoma cells. *J Biochem Mol Biol* 2005;38:167–176.

59. Hong F, Freeman ML, Liebler DC. Identification of sensor cysteines in human Keap1 modified by the cancer chemopreventive agent sulforaphane. *Chem Res Toxicol* 2005;18:1917–1926.

60. Keum YS, Yu S, Chang PP, Yuan X, Kim JH, Xu C, Han J, Agarwal A, Kong AN. Mechanism of action of sulforaphane: inhibition of p38 mitogen-activated protein kinase isoforms contributing to the induction of antioxidant response element-mediated heme oxygenase-1 in human hepatoma HepG2 cells. *Cancer Res* 2006;66:8804–8813.

61. Heiss E, Herhaus C, Klimo K, Bartsch H, Gerhauser C. Nuclear factor kappa B is a molecular target for sulforaphane-mediated anti-inflammatory mechanisms. *J Biol Chem* 2001;276:32008–32015.

62. Gamet-Payrastre L, Li P, Lumeau S, Cassar G, Dupont MA, Chevolleau S, Gasc N, Tulliez J, Terce F. Sulforaphane, a naturally occurring isothiocyanate, induces cell cycle arrest and apoptosis in HT29 human colon cancer cells. *Cancer Res* 2000;60:1426–1433.

63. Juge N, Mithen RF, Traka M. Molecular basis for chemoprevention by sulforaphane: a comprehensive review. *Cell Mol Life Sci* 2007;64:1105–1127.